ELSEVIER

Journal of Nuclear Materials 283–287 (2000) 827–831

journal of nuclear materials

www.elsevier.nl/locate/jnucmat

Annealing behavior of irradiation hardening and microstructure in helium-implanted reduced activation martensitic steel

A. Kimura [a,*], R. Kasada [a], R. Sugano [a], A. Hasegawa [b], H. Matsui [c]

[a] *Institute of Advanced Energy, Kyoto University, Uji, Kyoto 611-0011, Japan*
[b] *Department of Engineering, Tohoku University, Aramaki, Aoba, Sendai 980-0077, Japan*
[c] *Institute for Materials Research, Tohoku University, Sendai 980-0077, Japan*

Abstract

Post-implantation annealing behavior was investigated for a reduced activation martensitic steel (RAMS), which was homogeneously implanted with 580 at.ppm of helium by cyclotron utilizing energy degrader at below 429 K. Post-implantation isochronal annealing caused no age hardening but the gradual recovery of the hardening even above 673 K, while the neutron irradiated specimen showed a complete recovery of the hardening by the annealing above 673 K. Two-component analysis of positron lifetime measurements along with hardness measurements indicated that long lifetime component (τ_2) in the helium-implanted steel still existed after annealing up to 873 K. Evolution of helium bubbles during annealing was examined by TEM and it was revealed that helium bubbles tend to be formed at lath boundaries by the annealing above 723 K. Helium desorption was observed by the annealing above 773 K where recovery of the hardening began.

1. Introduction

Reduced-activation 7–9Cr martensitic steels (RAMSs) have been the prime candidate for structural materials in DEMO reactor and the beyond [1–3], where the transmutation helium-induced embrittlement has been considered to be one of the critical issues for reactor operation [4,5]. The previous works on helium effects from implantation and neutron irradiation experiments on high temperature (>673 K) deformation process emphasized that no marked ductility loss was observed for ferritic steels [6–9], although isotope/tailoring experiments suggest a potential degradation effect of helium [10–15]. More recently, authors investigated the effect of helium implantation on ductile–brittle transition temperature by means of small punch (SP) test technique and concluded that an implantation with helium up to 580 at.ppm at a temperature below 432 K resulted in no enhancement of shift in the SP-DBTT to high temperature [16–18]. High resistance to low temperature helium embrittlement of martensitic steel is considered to be due to high trapping capacity of its martensitic structure for helium atoms. It is, however, supposed that helium implantation at rather high temperatures would cause significant degradation of fracture toughness at low temperature because of evolution of helium bubbles during implantation. Post-implantation annealing may cause detrapping helium and growth of helium bubbles. Consequently, helium bubbles might degrade the fracture toughness at low temperature.

In this work, annealing behavior of helium-implanted RAMS is investigated to make clear the evolution process of helium bubbles and their effect on the hardness of the steel.

2. Experimental

Chemical compositions of RAMSs used in this study are shown in Table 1 with heat treatment conditions.

* Corresponding author. Tel.: +81-774 383 476; fax: +81-774 38 3479.
E-mail address: kimura@iae.kyoto-u.ac.jp (A. Kimura).

0022-3115/00/$ - see front matter
PII: S0022-3115(00)00090-8

Table 1
Chemical compositions and heat treatment conditions of RAMSs

	C	Si	Mn	P	S	Cr	W	V	Ta	Ti	B	Ni
JLM-1[a]	0.10	0.042	0.53	0.002	0.0014	9.03	2.06	0.26	0.051	0.021	0.0032	–
Mod.JLF-1[b]	0.10	0.01	0.01	0.004	0.0014	8.92	2.02	0.26	0.069	0.04	–	1.00

[a] JLM-1: normalized for 30 min at 1323 K (AC) and tempered for 1 h at 1033 K (AC).
[b] Mod.JLF-1: normalized for 30 min at 1323 K (AC) and tempered for 1 h at 973 K (AC).

The detail of helium implantation method was shown in elsewhere [16]. Helium was homogeneously implanted up to 120 and 580 at.ppm by using energy degrader wheels. The maximum displacement damage was estimated to be 0.048 and 0.226 dpa by the TRIM code calculation. The damage rate and the helium implantation rate were 8.7×10^{-7} dpa/s and 2.6×10^{3} at.ppm/dpa, respectively [16,17]. For comparison, neutron irradiation was performed in Japanese Materials Test Reactor (JMTR), where the damage rate and the helium implantation rate were 6.1×10^{-8} dpa/s and 9×10^{-2} at.ppm/dpa, respectively.

After the implantation and neutron irradiation, a pair of disc specimens were isochronally annealed from 423 to 873 K for 1 h at each step of 50 K for micro-Vickers hardness tests and positron annihilation lifetime (PA) measurements, which were performed at room temperature following annealing at each temperature. Hardness measurements were carried out with a load of 200 g. PA spectra were decomposed into two components, that is, a matrix component (τ_1, I_1) and a microvoid component (τ_2, I_2), where τ_i and I_i were the lifetime and intensity of ith component, respectively. After the annealing up to 873 K, one of discs was electrolitically polished for microstructure observation by transmission electron microscopy (TEM).

In order to investigate the evolution process of helium bubbles during annealing, an as-implanted disc was thinned then isochronally annealed for examination of microstructure following annealing at each temperature from 583 to 828 K. During the annealing, mass spectroscopy measurements were also performed under a vacuum of around 7×10^{-5} Pa.

3. Results

3.1. Micro-Vickers hardness measurements

Recovery behavior of micro-Vickers hardness by isochronal annealing is shown in Fig. 1 for helium-implanted steel along with that of neutron irradiated one. Neutron irradiation was performed in Japanese Materials Test Reactor (JMTR) up to a dose of 0.15 dpa at 493 K utilizing temperature-controlled capsule. As shown in the previous works [15,16], both the helium implantation-induced hardening and neutron-induced

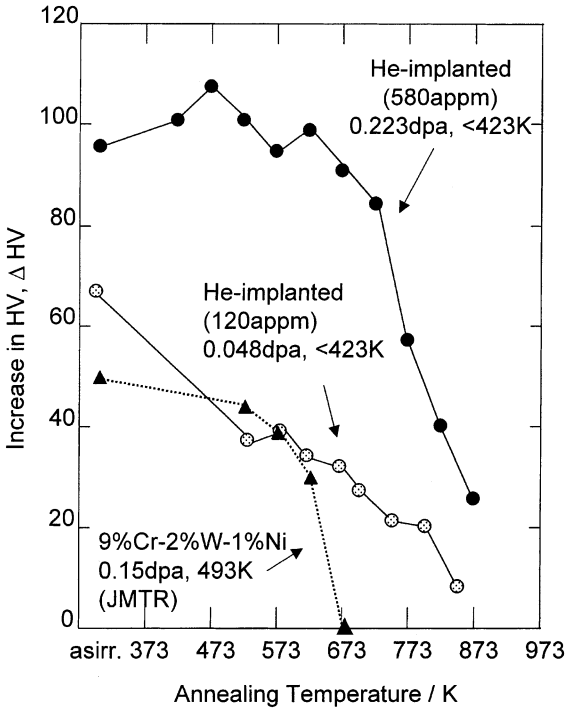

Fig. 1. The recovery behavior of irradiation hardening, ΔH_V, of helium-implanted JLM-1 by CYRIC and neutron irradiated Mod.JLF-1 in JMTR during isochronal (1 h) annealing from 423 to 873 K ($\Delta T = 50$ K).

hardening were well interpreted in terms of displacement damage. Recovery behavior of helium-implanted steel, however, is very different from that of neutron-irradiated one; the helium implantation-induced hardening still almost remained following the annealing to 673 K, while neutron-induced hardening completely diminished, and a large recovery stage appeared at around 623 and 723 K for neutron and helium implantation-induced hardening, respectively. It is worth to notice that no significant age hardening was observed but helium implantation-induced hardening still observed even after the annealing to 873 K.

3.2. Positron annihilation lifetime measurements

Annealing behaviors of positron lifetime and intensity of helium-implanted and neutron irradiated

steels are shown in Fig. 2. Neutron irradiation conditions are also shown in the figure. A long lifetime component, τ_2, is smaller in helium-implanted steel than neutron-irradiated one, suggesting that microvoids in helium-implanted steel are smaller in size than neutron-irradiated one [19]. Although helium may reduce the lifetime of positron in the microvoid [20], this mechanism has been considered to be unrealistic in the previous work [16]. The annealing behavior of neutron-irradiated steel is simple and appears to be related with the recovery behavior of the irradiation hardening; microvoids disappeared abruptly following annealing to 623 K where neutron-irradiation hardening began to recover. As for the steel implanted with 580 at.ppm of helium, a long lifetime component, namely microvoids, still existed following annealing to 623 K. Furthermore, subsequent annealing to higher temperature resulted in such a trend that size and density of microvoids increased with increasing annealing temperature up to 873 K.

3.3. TEM observations

Fig. 3 shows the microstructure of 580 at.ppm of helium-implanted steel after isochronal annealing up to 873 K. One of the pair of disc specimens, which were

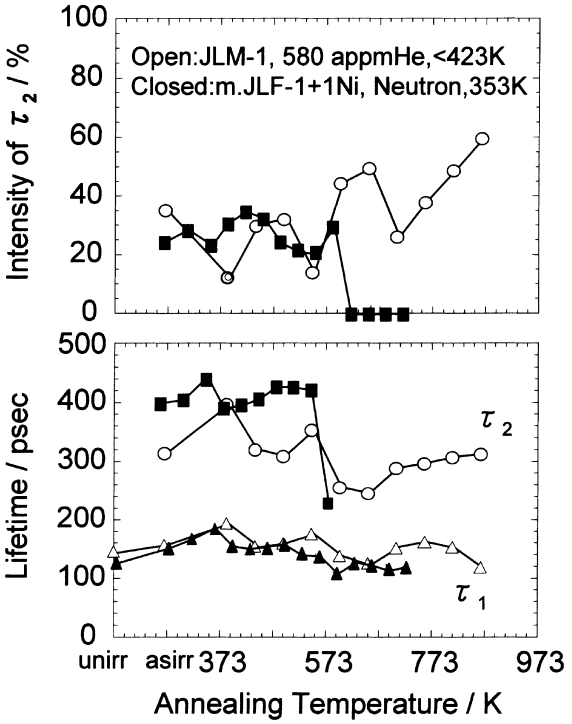

Fig. 2. The recovery behavior of PA parameters during isochronal annealing of helium-implanted JLM-1 (open symbols) and neutron-irradiated Mod.JLF-1 (closed symbols).

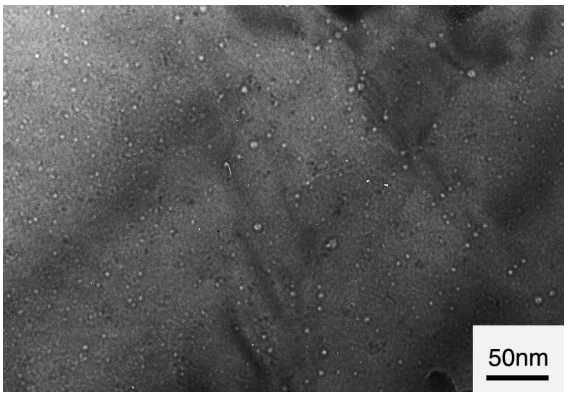

Fig. 3. The microstructure of 580 at.ppm of helium-implanted steel after isochronal (1 h) annealing from 423 to 873 K ($\Delta T = 50$ K).

used to measure positron lifetime but not for measurements of micro-Vickers hardness, was examined by TEM. As clearly shown in the figure, a number of bubbles were observed after the annealing. Since no bubbles was observed in neutron-irradiated and annealed up to 873 K in the same manner with the helium-implanted steel, the bubbles are considered to be helium bubbles. Also, since no helium bubbles were observed at as-implanted condition, these bubbles were considered to form during annealing up to 873 K. Nucleation sites of helium bubbles in RAMS are recognized to be dislocation, sub-grain (lath) boundaries and precipitate interfaces as shown in Fig. 3.

In order to determine the temperature where helium bubbles appear during annealing, a thinned TEM disc at as-implanted (580 at.ppm of helium) condition was isochronally annealed in the same manner, as is the above. Following annealing at each temperature, TEM examination was performed. Fig. 4 shows the microstructures of helium-implanted steel following annealing to 583, 723, 778 and 828 K. After annealing to 583 K, no cavity was observed. Some cavities appeared both at grain boundaries and in the matrix after annealing to 723 and 778 K. Annealing up to 823 K resulted in an increase in bubble size both at lath boundaries and in the matrix. No bubbles, however, existed in the specimen annealed up to 873 K at a thinned condition. This is inconsistent with the result obtained for the specimen thinned after the annealing up to 873 K, where a number of helium bubbles were observed. The interpretation will be given in the discussion section.

3.4. Helium desorption measurements

During annealing the thinned TEM specimen implanted with 580 at.ppm of helium, helium desorption measurements were carried out. Thermal desorption of

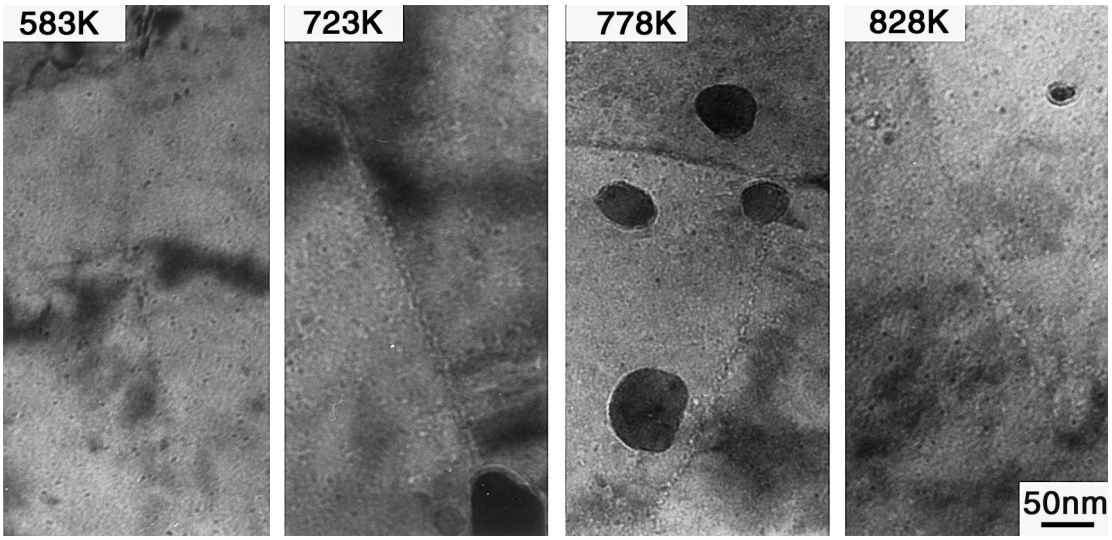

Fig. 4. The microstructures of 580 at.ppm of helium-implanted steel following annealing to 583, 723, 778 and 828 K (1 h). Thinned specimen was subsequently annealed at each temperature and then observed by TEM.

helium measured during annealing for 15 min at each temperature is shown in Fig. 5, where the out-gassing helium pressure, P^{He} (net), was defined as a subtraction of normalized back ground helium pressure, P^{BG}, from the measured helium pressure, P^{He} (measured), by the following relationship:

$$P^{He}_{net} = P^{He}_{measured} - \left(\frac{P^{Total}_{B.G.}}{P^{Total}_{He}}\right) P^{B.G.}_{measured}, \quad (1)$$

where P^{Total} is the total pressure during the measurement. As shown in the figure, a somewhat larger helium desorption occurred during annealing above 773 K showing a peak at 823 K and decrease with increasing annealing temperature to 923 K. Helium desorption appears to increase above 973 K.

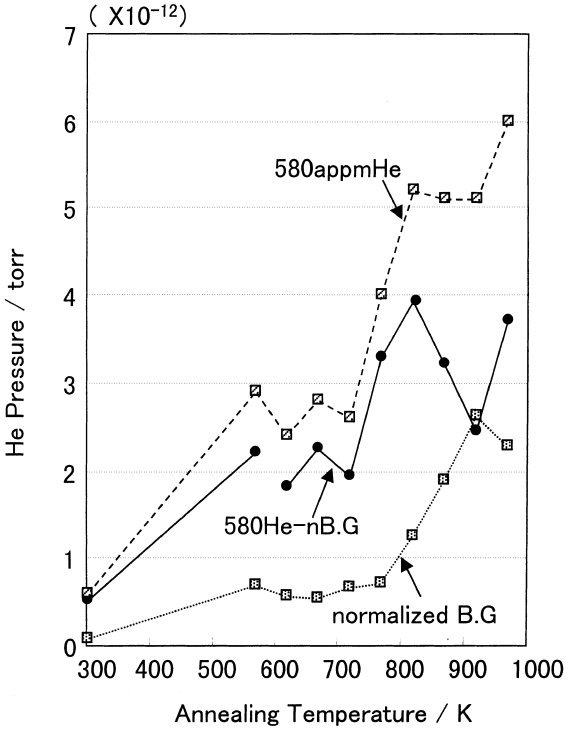

Fig. 5. Thermal desorption of helium from a thinned specimen measured during annealing for 15 min at each temperature.

4. Discussion

Neutron irradiation hardening of RAMs was usually observed after the irradiation below 693 K [2] where interstitial loops and microvoids were formed. Irradiation above 693 K resulted in no hardening in these steels because the defect clusters were unstable at those temperatures [2]. Retardation of the thermal recovery of the hardening in helium-implanted steel may be due to (1) helium bubbles that are stable above 693 K and could be obstacles for dislocation motion and/or (2) interstitial loops that can still exist above 693 K and cause the hardening by the overall effects from matrix and possibly lath boundaries. During the annealing from 723 to 873 K, the irradiation hardening reduced, while τ_2 and I_2 appeared to increase. If helium bubble were attributed for the hardening observed above 673 K, age hardening could be observed since the increase in the density of small helium bubbles increased hardness. Our previous study showed that there was no correlation between

hardness and PA parameters [21], indicating that microvoids were not the main cause of irradiation hardening. Instead, since helium bubbles are considered to be more thermally stable than voids without helium in it, thermal decomposition of microvoids, which may play a role in annihilation of small interstitial loops, was retarded and consequently the hardening remained. Helium desorption became significant at 773 K where the hardening began to reduce, which is also interpreted in terms of decomposition of helium bubbles; decomposition of helium bubbles causes an escape of helium out of specimen and vacancy annihilation at interstitial loop.

A series of TEM observation study during annealing revealed that helium bubble formation appears to occur at grain boundaries after annealing to 723 K and also in the matrix at 828 K, but not at 873 K. As mentioned before, a significant difference was observed between specimens annealed in bulky and thinned condition; a number of bubbles were observed in the former but not in the later at all. This may be attributed to specimen thickness effect on vacancy behavior; in the thinned specimen, vacancies and small bubbles [22] easily escape from specimen surfaces and prevent helium bubbles from growing up at high temperature, such as 873 K. At around 723 K, however, some helium was trapped at grain boundaries then grew up to the helium bubbles of visible size.

As clearly shown in the TEM photos, many helium bubbles were observed at dislocations, sub-grain boundaries and grain boundaries, indicating that implanted helium is dispersed at a lot of trapping sites in the martensitic structure. This results in suppression of aggregation of large amount of helium to form helium bubbles, which could degrade fracture toughness.

5. Summary

Post-helium implantation annealing caused no age hardening but the gradual recovery of the hardening even above 673 K, while the neutron irradiated specimen showed complete recovery of hardening by the annealing above 673 K. Positron lifetime measurements along with hardness measurements suggest that helium bubbles formed during annealing causes no hardening. Microstructure observation by TEM revealed that RAMS has a number of trapping sites for helium, to which a high resistance to helium embrittlement of RAMSs is considered to be attributed.

Acknowledgements

The authors are grateful to Professor K. Abe, graduate students in his laboratory, and CYRIC staff of Tohoku University for their help of helium implantation with a cyclotron. We would like to thank staff of Oarai branch, Institute for Materials Research, for utilizing hot laboratories.

References

[1] T. Morimura, A. Kimura, H. Matsui, J. Nucl. Mater. 239 (1996) 118.
[2] A. Kimura, M. Narui, T. Misawa, H. Matsui, A. Kohyama, J. Nucl. Mater. 258–263 (1998) 1340.
[3] A. Hishinuma, A. Kohyama, R.L. Klueh, D.S. Gelles, W. Dietz, K. Ehrlich, J. Nucl. Mater. 258–263 (1998) 193.
[4] H. Ullmaier, Nucl. Fus. 24 (8) (1984).
[5] H. Schroeder, J. Nucl. Mater. 155–157 (1988) 1032.
[6] A. Hasegawa, N. Yamamoto, H. Shiraishi, J. Nucl. Mater. 202 (1993) 266.
[7] A. Hasegawa, H. Shiraishi, H. Matsui, K. Abe, J. Nucl. Mater. 212–215 (1994) 720.
[8] H. Ullmaier, E. Camus, J. Nucl. Mater. 251 (1997) 262.
[9] U. Stamm, H. Schroeder, J. Nucl. Mater. 155–157 (1988) 1059.
[10] R.L. Klueh, D.J. Alexander, J. Nucl. Mater. 218 (1995) 151.
[11] D.S. Gelles, G.L. Hankin, M.L. Hamilton, J. Nucl. Mater. 251 (1997) 188.
[12] P.J. Maziasz, R.L. Klueh, ASTM STP 1046 (1989) 35.
[13] K. Shiba, M. Suzuki, A. Hishinuma, J.E. Pawel, ASTM STP 1270 (1996) 753.
[14] N. Wanderka, E. Camus, H. Wollenberger, Mat. Res. Soc. Symp. Proc. 439 (1997) 451.
[15] R. Lindau, A. Möslang, D. Preininger, M. Rieth, H.D. Rohrig, J. Nucl. Mater. 271–272 (1999) 450.
[16] A. Kimura, T. Morimura, R. Kasada, H. Matsui, A. Hasegawa, K. Abe, ASTM STP 1366 (2000) 626.
[17] R. Kasada, T. Morimura, A. Hasegawa, A. Kimura, J. Nucl. Mater., in press.
[18] R. Kasada, A. Kimura, H. Matsui, M. Narui, J. Nucl. Mater. 258–263 (1998) 1199.
[19] M.J. Puska, R.M. Nieminen, J. Phys. F 13 (1983) 333.
[20] K.O. Jensen, R.M. Nieminen, Phs. Rev. B. 35 (4) (1987) 2087.
[21] R. Kasada, A. Kimura, H. Matsui, ASTM STP 1366, in press.
[22] Z.H. Luklinska, G. von Bradsky, P.J. Goodhew, J. Nucl. Mater. 135 (1985) 206.